OPTICAL PROPERTIES OF ZnS NANOPARTICLES PRECIPITATED AT VARIOUS MOLAR RATIOS OF SULPHIDE AND ZINC IONS AND STABILIZED BY CTAB

ONDŘEJ KOZÁK[a], PETR PRAUS[b*], RICHARD DVORSKÝ[c]
[a]Regional Materials Science and Technology Centre, VŠB-Technical University of Ostrava, 17. listopadu 15, 708 33 Ostrava-Poruba, Czech Republic
[b]Department of Analytical Chemistry and Material Testing, VŠB-Technical University of Ostrava, 17. listopadu 15, 708 33 Ostrava-Poruba, Czech Republic
[c]Institute of Physics, VŠB-Technical University of Ostrava, 17. listopadu 15, 708 33 Ostrava-Poruba, Czech Republic

ZnS nanoparticles were precipitated by the reaction of zinc and sulphide ions in aqueous media and stabilized by cetyltrimethylammonium bromide (CTAB). The nanoparticles size (diameter) was calculated using the relationship between band-gap energy and radius as a result of the quantum size effect. Depending on the molar ratio of precursors S^{2-}/Zn^{2+} = 0.25–2.0 and time elapsed from their preparation t = 0–5 h, nanoparticles with sizes of 3.5–4.8 nm were obtained. The absorption of UV radiation and photoluminescence (PL) of the nanoparticles dispersions were studied. The nanoparticles growth dependent on time and the S^{2-}/Zn^{2+} ratio were indicated by changes in UV absorption and PL spectra. The stabilization effect of CTAB was observed for all S^{2-}/Zn^{2+} ratios up to 5 hours. At longer time intervals (3 a 4 days) flocs of ZnS nanoparticles and CTAB were observed.

1. Introduction

Semiconductor nanoparticles such as ZnS have been in the scope of many research works over the last decade. The reasons for such a great attention are their outstanding physical and chemical properties, which differ considerably from that of bulk ZnS. The enhanced properties make the nanoparticles very utilizable in the field of chemical industry, semiconductor technology, optical devices, medicine, environment protection etc. [1-3].

ZnS nanoparticles are mostly prepared by precipitation [4-7], which involves the reaction between zinc and sulphide precursors. Their concentration and stoichiometric ratio plays an important role in the properties of nascent nanoparticles. Several studies mentioning the dependence of ZnS nanoparticle size upon the molar ratio of precursors have been published [8-10].

Various ways to prevent ZnS nanoparticles from unrestricted growth in aqueous media have been described in the literature. A whole range of organic compounds can serve as stabilizers, however surfactants are among the most used ones [11-13]. Surfactants such as cetyltrimethylammonium bromide (CTAB) form micelles in aqueous media if their critical micellar concentration (CMC) is exceeded. The nascent particles can be capped inside these micelles and thus protected from unlimited growth [11,14].

In general, one of the promising features of semiconductor nanoparticles is their photoluminescence. Many studies dealt with PL of both pure ZnS [15] and ZnS doped with different metals ions such as Mn^{2+} [16], Ag^+ [17], Fe^{2+} [18] and others [19]. It was shown that the

---

* Corresponding autor: petr.praus@vsb.cz

molar ratio of S^{2-}/Zn^{2+} has an influence on the PL intensity of both undoped [10] and doped [8] ZnS nanoparticles. Mehta and Kumar [20] suggested that the PL intensity is time-dependent, which was also supported by Sato et al. [21] and their study of CdS photoluminescence.

The aim of this work was to study the size. UV absorption and photoluminescence properties of ZnS nanoparticles dependent on the S^{2-}/Zn^{2+} molar ratio and time elapsed from their preparation. CTAB was used for their stabilization.

2. Experimental

The used chemicals were of analytical reagent grade: Zinc acetate, sodium sulphide (Lachema, Czech Republic), cetyltrimethylammonium bromide (Sigma Aldrich). The water used for aqueous solutions preparation was deionized by reverse osmosis (Aqua Osmotic, Czech Republic). The ZnS nanoparticles were prepared in the presence of CTAB following the method described in our previous work [22]. The aqueous solution of Na_2S and CTAB (solution A) was added to the stirred aqueous solution of zinc acetate (solution B). A set of the solutions A with the different Na_2S concentration was used while the concentration of CTAB and zinc precursor was kept constant. The molar ratio S^{2-}/Zn^{2+} was changed from 0.25 to 2.0 and the concentration of Zn^{2+} was constant. Properties of the ZnS nanoparticles were measured in freshly prepared dispersions and in the same dispersions after different periods of time during which the dispersion were exposed to day light and air atmosphere in covered beaker (to minimize vaporisation).

UV-VIS spectra of the ZnS dispersions were measured by an UV-VIS spectrometer Lambda 35 (Perkin Elmer, USA) using 1 cm quartz cuvettes. Photoluminescence spectra were recorded at room temperature by a FLS900 fluorescence spectrometer (Edinburgh Instruments, UK) at the excitation wavelength of 315 nm using 1 cm quartz cuvettes. The pH value of the ZnS dispersions was measured by means of a Metrohm pH meter 691 (Metrohm, Switzerland).

Transmission electron microscopy of the ZnS dispersions was performed on a Jeol JEM 1230 microscope operated at 80 kV. The prepared samples of the ZnS nanoparticles stabilized by CTAB were placed on a copper grid (400 mesh) coated by a film of 1.5–3.0 wt. % of polyvinylformaldehyde in chloroform, dried by blotting paper and analyzed after 2 days. The contrast of micrographs was improved by 1wt. % solution of ammonium molybdate added to the samples. The X-ray powder diffraction (XRD) study was performed by a powder diffractometer (BRUKER D8 ADVANCE) equipped with scintillation and position-sensitive detectors (VANTEC) and a source of CoKα radiation. The diffraction patterns were recorded in an ambient atmosphere under constant conditions (50 kV, 60 mA). The XRD patterns were identified using the PDF-2-Release 2004 database.

3. Results and discussion

ZnS nanoparticles were precipitated at different S^{2-}/Zn^{2+} ratios in the presence of stabilizing CTAB. The absorption and photoluminiscence spectra of the ZnS dispersions were recorded.

3.1 UV-VIS absorption spectrometry

The solutions A and B were mixed together and the UV spectra of the originating ZnS dispersions were recorded. The time elapsed between mixing the solutions A and B to recording the first UV spectrum (ref. to $t = 0$ h) was approximately 30 seconds. The prepared dispersions were then kept unstirred in covered beakers under room conditions and the other spectra were recorded after 1, 3, and 5 hours.

The UV spectra recorded at $t = 0$ h and $t = 5$ h can be seen in Figure 1. Compared to bulk ZnS having the absorption edge at about 340 nm [23], the blue-shifted absorption edges observed at 310 nm confirmed formation of the nanoparticles. In Fig. 1A one can see that with the increasing S^{2-}/Zn^{2+} ratio in the range of 0.25–1.25 there is a huge growth of the absorbance

shoulder. This was caused by the higher concentration of the formed ZnS nanoparticles and very likely by scattering of the UV radiation on flocs of the ZnS and CTAB that were observed by TEM (see below). Increasing the ratio above 1.25 caused no significant absorbance increase, which means that the concentration of the ZnS nanoparticles remained nearly constant.
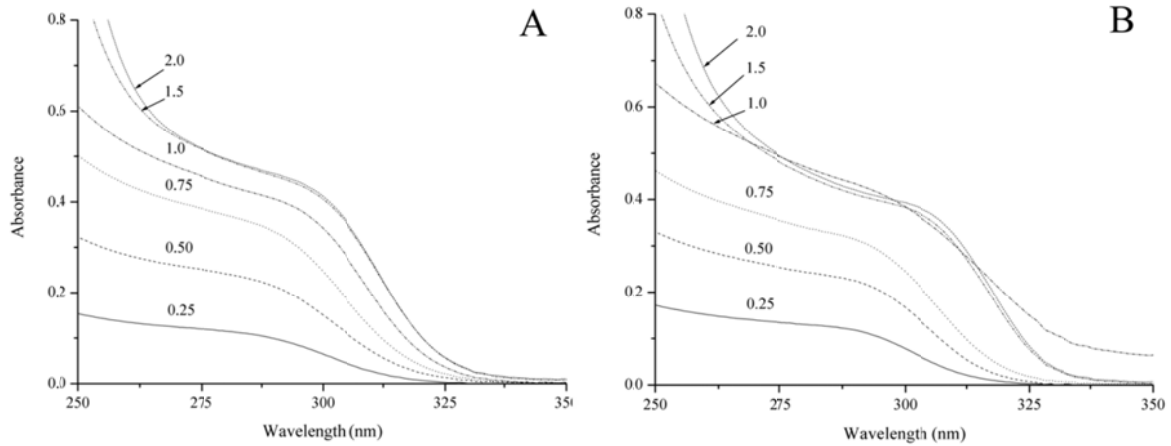
Fig. 1 Absorption spectra of ZnS dispersion just after precipitation (A) and 5 hours (B)

Comparing the absorption spectra recorded right after the ZnS preparation (Fig. 1A) and after 5 hours (Fig. 1B) it is obvious that there is a slight red-shift of all spectra suggesting that the size of the nanoparticles increased. There is also obvious a deformation of absorbance spectra and increase of the absorbance background at e.g. 350 nm for the dispersions prepared at $S^{2-}/Zn^{2+} = 1.0–2.0$. This was also observable with the naked eye as an increase in the turbidity of the ZnS dispersions.

The UV absorption spectra were deconvoluted by their fitting with three overlapping Gaussian curves and one exponential curve as suggested by Tiemann et al. [24] in order to extract the first excitonic absorption band. The red-shifts of its absorption maxima from 287 nm to 308 nm in the dependence on the S^{2-}/Zn^{2+} ratios and time (up to 5 hours) indicated the nanoparticles growth due to the Ostwald ripening process.

3.1.2 Calculation of ZnS nanoparticle size

The mean size of ZnS nanoparticles was calculated from the band-gap energy using the relationship (Eq. 1) describing the quantum size effect [25] as follows

$$E_{bg}(nano) = E_{bg}(bulk) + \frac{h^2}{8r^2}\left(\frac{1}{m_e} + \frac{1}{m_h}\right) - \left(\frac{1.8e^2}{4\pi\varepsilon_r\varepsilon_0 r}\right) \qquad (1)$$

where $E_{bg}(nano)$ and $E_{bg}(bulk)$ are the band gap energies of bulk and nano ZnS, respectively, h is the Planck´s constant, r is the radius of the nanoparticle, m_e and m_h are the effective masses of electron and hole respectively and ε_r is the relative permittivity dielectric constant of the material, ε_o is the permittivity of vacuum. Here, $m_e = 0.42m_0$ and $m_h = 0.6m_0$, where m_0 is the free electron mass and $\varepsilon_r = 8.76$ [26]. The band-gap energy was obtained by the construction of the Tauc plot [27] as already described in our previous works [14,22]. The dependence of the mean ZnS nanoparticle size upon the S^{2-}/Zn^{2+} ratio and the time is demonstrated in Fig. 2.
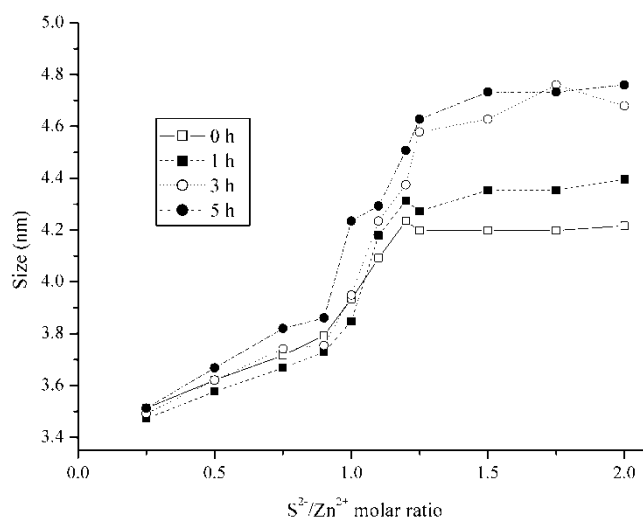
Fig. 2 Dependence of ZnS nanoparticles size on molar S^{2-}/Zn^{2+} ratio

At all tested time intervals the nanoparticle size increased until $S^{2-}/Zn^{2+} = 1.25$ as a result of increasing amount of ZnS. It is obvious that the nanoparticles growth was finished during the first 3 hours. The nanoparticles were not coagulated by two main reasons. First, according to the Weimarn's law the lower concentration of S^{2-} means that the ZnS concentration was small and the nanoparticles were less exposed to direct interactions leading to coagulation. Second, the excessive Zn^{2+} ions were adsorbed on the nanoparticles surface according to the Paneth-Fajans rule forming the electric bilayers of Zn^{2+} and acetic anions, which stabilized the ZnS dispersion by mean of electrostatic repulsion. In addition, CTAB also played an important role in the stabilization. Unlike the situation studied recently [14], when CTA ions were adsorbed by their positive headgroups to ZnS nanoparticles surface covered by excess S^{2-} ions, in this case the CTA ions were adsorbed on the nanoparticles (covered by Zn^{2+} ions) likely by means of their hydrophobic alkyl chains. Thus, the surface positive charge was balanced by bromide and acetate ions resulting in miceles that were mutually stabilized by electrostatic repulsion forces. The nanoparticle growth in time was caused by the Ostwald ripening.

At S^{2-}/Zn^{2+} ratio < 1.25 pH varied in the range of 6−7 and sulphide also existed in the forms of H_2S and HS^- that were unavailable to form ZnS. This is the reason why the maximum size of ZnS was reached at $S^{2-}/Zn^{2+} = 1.25$ and not at their theoretical stoichiometry equals to 1. Also, the huge change of pH of the formed ZnS nanodispersion from 6 ($S^{2-}/Zn^{2+} = 1$) to 10.4 ($S^{2-}/Zn^{2+} = 1.25$) implies that a slight excess of sulphur precursor is required to reach the stoichiometric amount of S^{2-} ions and thus to get to the constant particle size.

At $S^{2-}/Zn^{2+} \geq 1.25$ size of the ZnS nanoparticles remained nearly constant due to the lack of Zn^{2+} to form other ZnS. The excessive S^{2-} ions were adsorbed on the nanoparticles surface forming the electric bilayer with CTAB as mentioned above [14]. The nanoparticle growth caused by the Ostwald ripening was more intensive then at $S^{2-}/Zn^{2+} < 1.25$.

3.2 Transmission electron microscopy

Transmission electron microscopy was performed to study the stabilization effect of CTAB on the ZnS nanoparticles. Figure 3 shows the TEM micrograph of ZnS and CTAB dispersion prepared at $S^{2-}/Zn^{2+} = 2$ and $t = 0$ h. It is obvious that both the separated (on background) and flocculated ZnS nanoparticles are present in the dispersion right after the synthesis. The discrete ZnS nanoparticles can be distinguished in the flocs, which agrees with the fact that the nanoparticles absorbed the UV radiation of the lower wavelengths than bulk ZnS as discussed above. ZnS and CTAB were identified by XRD as main crystalline phases.
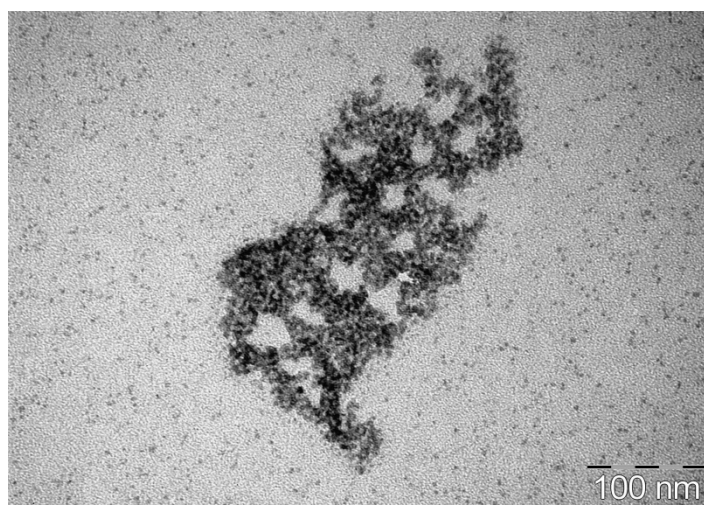
Fig. 3 TEM micrograph of ZnS and CTAB dispersion at $S^{2-}/Zn^{2+} = 2$ at $t = 0$ h

3.3 Luminescence spectroscopy

There is a strong relation between optical absorption properties of semiconductor materials and their photoluminescence. Absorption of energy equals to or higher than the band-gap energy is required for subsequent photoemission. Unless the photo–excited electron-hole pair (exciton) undergoes nonradiative recombination, an emission of photon can occur. The quantum size effect influences both the position and shape of the emission and excitation bands in the PL spectra.
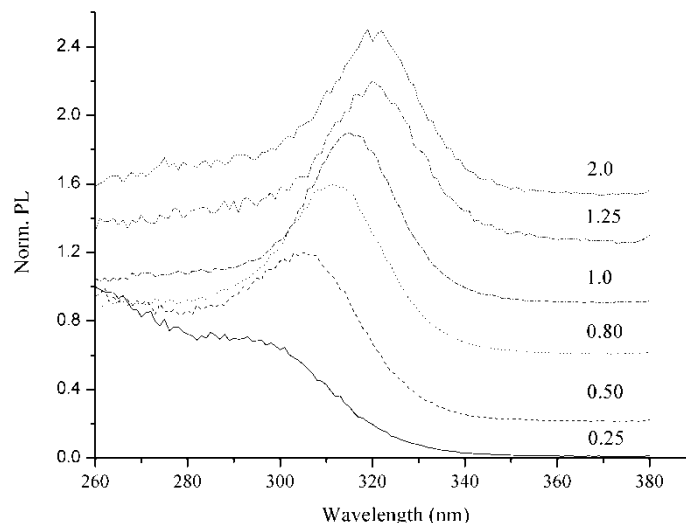
Fig. 4 Excitation PL spectra of ZnS dispersions at various S^{2-}/Zn^{2+} ratios

When the size of semiconductor nanoparticles is getting closer to the Bohr exciton radius a blue-shift in the absorption or excitation PL spectra [28] as a result of the quantum size effect.

The excitation PL spectra of the ZnS dispersions measured at 445 nm can be seen in Figure 4. The spectra were normalized and vertically shifted for clarity. The low-energy edge was red-shifted with increasing the S^{2-}/Zn^{2+} ratio until the stoichiometric ratio of 1.25 was reached. This observation agrees well with the red-shift absorption bands in Figure 1 and documents that lower energy was required to induce photoluminescence in dependence of the nanoparticle growth.

The PL spectra of the ZnS dispersions prepared at $S^{2-}/Zn^{2+} = 0.5$ in Figure 5A show the PL intensity and spectra shape dependence on the time elapsed from the ZnS precipitation. The increase of the PL intensity was observed as a result of the increase of concentrations of the ZnS

nanoparticles. The presence of a broad blue emission band suggests the defect ZnS structure with sulphur and zinc vacancies. Several ways of irradiative energy transfer can contribute to photoluminescence: the transitions from the conduction band to interstitial sulphur or zinc vacancies and from these vacancies to the valence band [11,17,29-31]. Generally, unlike bulk materials, nanoparticles show very broad PL bands due to larger band-gap energies, which enable excitons to recombine irradiatively at various states with the broader range of energies. Moreover, the presence of nanoparticles with different sizes (thus different band-gaps) broadens the PL band [32].
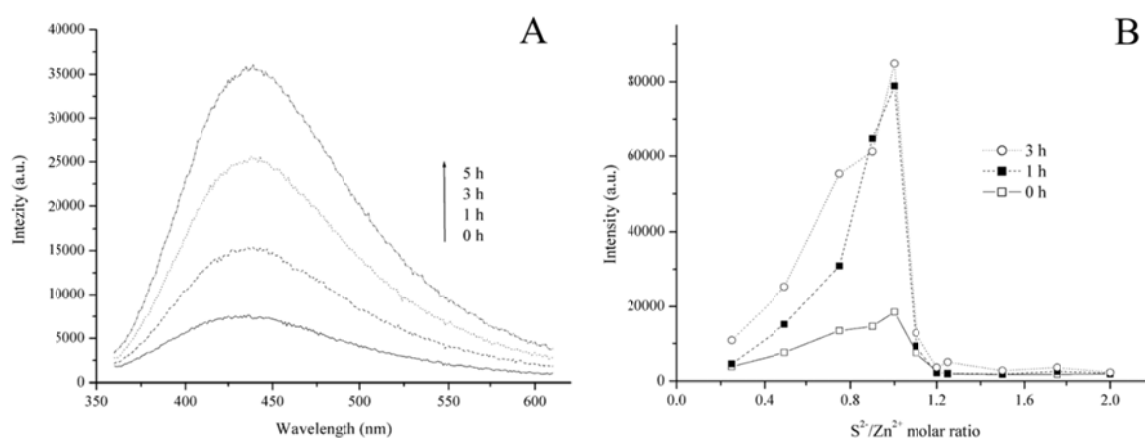
Fig. 5 Photoluminescence spectra of ZnS dispersion. (A) PL intensities at S^{2-}/Zn^{2+} = 0.5 and (B) maximal intensities against S^{2-}/Zn^{2+} at different time of growth (B)

At S^{2-}/Zn^{2+} = 2.0 the PL spectra were very similar but the PL intensity was an order of magnitude lower than at S^{2-}/Zn^{2+} = 0.5. This indicates that the excessive sulphide ions decreased the concentration of sulphide vacancies acting as luminescent centres.

To document the PL intensity changes with the S^{2-}/Zn^{2+} molar ratio and time a plot is shown in Figure 5B. In the region of S^{2-}/Zn^{2+} < 1.25, the PL intensity increased with the increasing S^{2-}/Zn^{2+} ratio, which corresponds to the increasing absorbance (concentration) of the ZnS nanoparticles (Fig. 1A). When the S^{2-}/Zn^{2+} ratio approached 1.25 the PL intensity reached maxima since the concentration of luminescent nanoparticles was also maximal. When the molar concentration of sulphide ions exceeded the stoichiometric one the PL intensity decreased due to reduction of the sulphide vacancies concentration.

4. Conclusion

In this study, the ZnS nanoparticles were precipitated at different S^{2-}/Zn^{2+} molar ratios in the presence of CTAB. Their sizes were calculated from the band-gap energies estimated from the UV absorption spectra. The nanoparticles growth was sensitively indicated by the changes in their UV absorption and PL spectra as a function of the time elapsed from their precipitation and the S^{2-}/Zn^{2+} ratio. It was observed that with the increasing S^{2-}/Zn^{2+} ratio up to 1.25, the particle size increased from 3.5 nm to 4.8 nm and then remained nearly constant. The most considerable growth of size was observed at S^{2-}/Zn^{2+} ≥ 1.25 since the maximum amount of ZnS was precipitated. The TEM study revealed that the ZnS nanoparticles formed flocs consisting of discrete nanoparticles and CTAB. The PL spectra indicated the lack of S^{2-} ions (i.e. S^{2-} vacancies) causing the intense defect-related blue photoluminescence, which considerably increased due to the nanoparticles growth. Further, the PL intensity decreased due to the excess of S^{2-} ions resulting in decrease of the concentration of the of S^{2-} vacancies.

It is of great importance to study the optical properties of ZnS nanoparticles in dispersions or powdered nanocomposites, to investigate their size, structure and stability. The next research will be focused on the stabilization of ZnS nanoparticles by CTAB at S^{2-}/Zn^{2+} < 1.25 using

molecular modelling methods [14]. Their photocatalytic properties will be tested for the photodecomposition of some environmental pollutants.

Acknowledgement

References

[1] D. Beydoun, R. Amal, G. Low, J. Nanopart. Res. **1**, 439 (1999).
[2] L. Shaoqin, T. Zhiyong, J. Mater. Chem. **20**, 24 (2010).
[3] F. Antolini, A. Ghezelbash, C. Esposito, E. Trave, L. Tapfer, B. Korgel, Mater. Lett. **60**, 1095 (2006).
[4] S.K. Mehta, S. Kumar, S. Chaudhary, K. K. Bhasin, M. Gradzielski, Nanoscale Res. Lett. **4**, 17 (2009).
[5] Z. Y. Ren, H. Yang, L. C. Shen, S. D. Han, J. Mater. Sci.: Mater. Electron. **19**, 1 (2008).
[6] D. Saenger, G. Jung, M. Mennig, J. Sol-Gel Sci. Technol. **13,** 635 (1998).
[7] Y. Li, X. He, M. Cao, Mater. Res. Bull. **43**, 3100 (2008) 3100.
[8] J. F. Suyver, S. F. Wuister, J. J. Kelly, A.Meijerink, Nano Let. **1**, 429 (2001).
[9] G. A. Martínez-Castañón, J. R. Martínez-Mendoza, F. Ruiz, J. González-Hernández, Inorg. Chem. Commun. **10**, 531 (2007).
[10] Q. Huang, L. Li, J. Xu, X. Zhang, G. Zhang, R. Xuan, Optoelectron. Lett. **6**, 161 (2010).
[11] S. K. Mehta, S. Kumar, M. Gradzielski, J. Colloid Interface Sci. 360 (2011) 497.
[12] P. Calandra, M. Goffredi, V.T. Liveri, Colloids Surf. A **160**, 9 (1999).
[13] T. Mthethwa, V. S. R. R. Pullabhotla, P. S. Mdluli, J. Wesley-Smith, N. Revaprasadu, Polyhedron **28**, 2977 (2009).
[14] P. Praus, R. Dvorský, P. Horínková, M. Pospíšil, P. Kovář, J. Colloid Interf. Sci. **377**, 58 (2012).
[15] Chatterjee, A. Priyam, S. C. Bhattacharya, A. Saha, Colloids Surf. A **297** (2007) 258.
[16] X. Ma, J. Song, Z. Yu, Thin Solid Films **519** (2011) 5043.
[17] A. Murugadoss, A. Chattopadhyay, Bull. Mater. Sci. **31**, 533 (2008).
[18] L. Liu, R. Xie, L. Yang, D. Xiao, J. Zhu, Phys. Status Solidi A **208**, 863 (2011).
[19] P. Yang, M. Lü, D. Xü, D. Yuan, G. Zhou, Chem. Phys. Lett. **336**, 76 (2001).
[20] S. K. Mehta, S. Kumar, J. Lumin. **130**, 2377 (2010).
[21] K. Sato, S.Kojima, S. Hattori, T. Chiba, K. Ueda-Sarson, T. Torimoto, Y. Tachibana, S. Kuwabata, Nanotechnology **18**, 465702 (2007).
[22] O. Kozák, P. Praus, K. Kočí, M. Klementová, J. Colloid Interface Sci. **352**, 244 (2010).
[23] M. K. Naskar, A. Patra, M. Chatterjee, J. Colloid Interface Sci. **297**, 271 (2006).
[24] M. Tiemann, Ö. Weiss, J. Hartikainen, F. Marlow, M. Lindén, ChemPhysChem **6**, 2113 (2005).
[25] L. E. Brus, J. Chem. Phys. **80**, 4403 (1984).
[26] K. Dutta, S. Manna, S.K. De, Synth. Met. **159**, 315 (2009).
[27] J. Tauc, in: J. Tauc (Ed.), Amorphous and Liquid Semiconductors, Plenum Press, New York (1974).
[28] H. Hu, W. Zhang, Opt. Mater. **28**, 536 (2006).
[29] P.H. Borse, N. Deshmukh, R.F. Shinde, S.K. Date, S.K. Kulkari, J. Mater. Sci. **34** 6087 (1999).
[30] K. Manzoor, S. R. Vadera, N. Kumar, T. R. N. Kutty, Mater. Chem. Phys. **82**, 718 (2003).
[31] W. Q. Peng, G. W. Cong, S. C. Qu, Z. G. Wang, Opt. Mater. **29**, 313 (2006).
[32] K. V. Anand, M. K. Chinnu, R. M Kumar, R. Mohan, R. Jayavel, J. Alloys Compd. **496**, 665 (2010).